

Illuminating gas in-/outflows in the MUSE deepest fields: discovery of Ly α nebulae around forming galaxies at $z \simeq 3.3$

E. Vanzella^{1*}, I. Balestra^{2,3}, M. Gronke⁴, W. Karman⁵, G.B. Caminha⁶,
M. Dijkstra⁴, P. Rosati⁶, S. De Barros^{1,7}, K. Caputi⁵, C. Grillo⁸, P. Tozzi⁹,
M. Meneghetti¹, A. Mercurio¹⁰, R. Gilli^{1†}

¹INAF – Osservatorio Astronomico di Bologna, via Ranzani 1, 40127 Bologna, Italy

²University Observatory Munich, Scheinerstrasse 1, 81679 Munich, Germany

³INAF – Osservatorio Astronomico di Trieste, via G. B. Tiepolo 11, I-34143, Trieste, Italy

⁴Institute of Theoretical Astrophysics, University of Oslo, Postboks 1029 Blindern, NO-0315 Oslo, Norway

⁵Kapteyn Astronomical Institute, University of Groningen, Postbus 800, 9700 AV Groningen, The Netherlands

⁶Dipartimento di Fisica e Scienze della Terra, Università di Ferrara, via Saragat 1, 44122 Ferrara, Italy

⁷Observatoire de Genève, Université de Genève, 51 Ch. des Maillettes, 1290, Versoix, Switzerland

⁸Dark Cosmology Centre, Niels Bohr Institute, University of Copenhagen, Juliane Maries Vej 30, DK-2100 Copenhagen, Denmark

⁹INAF – Osservatorio Astrofisico di Arcetri, Largo E. Fermi, I-50125, Firenze, Italy

¹⁰INAF – Osservatorio Astronomico di Capodimonte, Via Moiariello 16, I-80131 Napoli, Italy

ABSTRACT

We report on the discovery of extended Ly α nebulae at $z \simeq 3.3$ in the Hubble Ultra Deep Field (HUDF, $\simeq 40 \text{ kpc} \times 80 \text{ kpc}$) and behind the Hubble Frontier Field galaxy cluster MACSJ0416 ($\simeq 40 \text{ kpc}$), spatially associated with groups of star-forming galaxies. VLT/MUSE integral field spectroscopy reveals a complex structure with a spatially-varying double peaked Ly α emission. Overall, the spectral profiles of the two Ly α nebulae are remarkably similar, both showing a prominent blue emission, more intense and slightly broader than the red peak. From the first nebula, located in the HUDF, no X-ray emission has been detected, disfavoring the possible presence of AGNs. Spectroscopic redshifts have been derived for 11 galaxies within $2''$ from the nebula and spanning the redshift range $1.037 < z < 5.97$. The second nebula, behind MACSJ0416, shows three aligned star-forming galaxies plausibly associated to the emitting gas. In both systems, the associated galaxies reveal possible intense rest-frame-optical nebular emissions lines [O III] $\lambda\lambda 4959, 5007 + \text{H}\beta$ with equivalent widths as high as 1500 \AA rest-frame and star formation rates ranging from a few to tens of solar masses per year. A possible scenario is that of a group of young, star-forming galaxies sources of escaping ionising radiation that induce Ly α fluorescence, therefore revealing the kinematics of the surrounding gas. Also Ly α powered by star-formation and/or cooling radiation may resemble the double peaked spectral properties and the morphology observed here. If the intense blue emission is associated with inflowing gas, then we may be witnessing an early phase of galaxy or a proto-cluster (or group) formation.

Key words: galaxies: evolution – galaxies: distances and redshifts – galaxies: star-burst – gravitational lensing: strong

1 INTRODUCTION

Exchanges of gas between galaxies and the ambient intergalactic medium play an important role in the formation and evolution of galaxies. Circumgalactic gas at high redshift ($z > 3$) has been observed through absorption line studies using background sources close to foreground galax-

* E-mail: eros.vanzella@oabo.inaf.it

† Based on observations collected at the European Southern Observatory for Astronomical research in the Southern Hemisphere under ESO programmes P096.A-0045 and P094.A-0115.

ies (e.g., Lanzetta et al. 1995; Chen et al. 2001; Adelberger et al. 2003; Steidel et al. 2010; Giavalisco et al. 2011; Turner et al. 2014). The presence of a significant amount of circumgalactic gas has also been revealed through the detection of extended Ly α emission at several tens kpc scales around single galaxies ($L_{\alpha} \simeq 10^{42} \text{ erg s}^{-1}$, e.g., Steidel et al. 2010; Caminha et al. 2015; Patrício et al. 2016; Wisotzki et al. 2016) and up to hundreds of kpc scale around QSOs and/or high redshift radio galaxies ($L_{\alpha} \simeq 10^{44} \text{ erg s}^{-1}$, e.g., Borisova et al. 2016; Cantalupo et al. 2014; Swinbank et al. 2015).

While the origin of the extended Ly α emission is still debated, it is clear that the circumgalactic gas must be at least partly neutral. Extended Ly α emission is therefore a viable tool to investigate the presence, status and dynamics of the surrounding hydrogen gas, from single galaxies or galaxy groups. Various processes can be investigated, e.g., (1) the search for outflowing/inflowing material provide insights about feeding mechanism for galaxy formation and regulation on galactic baryonic/metal budgets and connection with the IGM, and (2) indirect signature of escaping ionizing radiation that illuminate inflowing/outflowing neutral hydrogen gas shaping the Ly α emission profile. The latter is connected with ionization capabilities of sources on their local environment (Rauch et al. 2011, 2016).

The extent of Ly α nebula is found to be strongly related to the luminosity of a central source, with the largest nebulae extending to hundreds of kpc around luminous AGN (e.g., Borisova et al. 2016; Swinbank et al. 2015; Cantalupo et al. 2014; Hennawi et al. 2015). The shape of these nebulae is often found to be symmetrical or filamentary around a central source (e.g., Hayes et al. 2011; Wisotzki et al. 2016; Patrício et al. 2016), where more luminous sources show more circular morphologies. The central source is in agreement with proposed mechanisms responsible for extended emission, however, there are nebulae where no central source is detected (Prescott et al. 2012).

The diverse origin of LABs can also be seen in the dynamics of Ly α nebulae. Most of the studied LABs have a chaotic distribution of Ly α emission (e.g., Christensen et al. 2004; Caminha et al. 2015; Prescott et al. 2012; Patrício et al. 2016; Francis et al. 2013) which is in agreement with Ly α scattering or an ionising central source as the origin of the extended emission. The discovery of rotating LABs (e.g., Prescott et al. 2015; Martin et al. 2015) indicates that also cold accretion flows can be responsible for extended Ly α emission.

In this work we report on two very similar systems at approximately the same redshift ($z = 3.3$) discovered in two different fields: one recently observed with long-list spectroscopy by Rauch et al. (2011, 2016) in the Hubble Ultra Deep Field (HUDF, hereafter), and a second one discovered as a multiply imaged system in the Hubble Frontier Fields cluster MACSJ0416. Both of these systems have been observed with VLT/MUSE integral field spectroscopy, which revealed extended Ly α emission coincident with a group of star-forming galaxies. We present a study of morphology and spectral profile of these systems, possibly tracing outflowing and inflowing gas.

In the following discussion we assume a flat cosmology with $\Omega_m = 0.3$, $\Omega_{\Lambda} = 0.7$ and $H_0 = 70 \text{ km s}^{-1} \text{ Mpc}^{-1}$, corresponding to 7.6 kpc proper for $1''$ separation at $z = 3.3$.

Table 1. List of parameters

Ly α nebula - HUDF	
Right ascension(J2000):	03h32m39.0s
Declination(J2000):	$-27^{\circ}46'17.0''$
Redshift(blue,red):	3.3172,3.3266 (± 0.0006)
L(Ly α) blue (erg s^{-1}):	$(5.5 \pm 0.1) \times 10^{42} \text{ erg s}^{-1}$
L(Ly α) red (erg s^{-1}):	$(4.0 \pm 0.1) \times 10^{42} \text{ erg s}^{-1}$
Possible galaxy counterparts	
#2-16373(SFR; Mass)	$4M_{\odot} \text{ yr}^{-1}; 2.9 \times 10^7 M_{\odot}$
#3-16376(SFR; Mass)	$46M_{\odot} \text{ yr}^{-1}; 1.2 \times 10^9 M_{\odot}$
#4-16148(SFR; Mass)	$0.1M_{\odot} \text{ yr}^{-1}; 5.5 \times 10^8 M_{\odot}$
#6-16330(SFR; Mass)	$2M_{\odot} \text{ yr}^{-1}; 3.2 \times 10^7 M_{\odot}$
#10-16506(SFR; Mass)	$100M_{\odot} \text{ yr}^{-1}; 9.0 \times 10^8 M_{\odot}$
Ly α nebula - MACSJ0416	
Right ascension(J2000)[A]:	04h16m10.9s
Declination(J2000)[A]:	$-24^{\circ}04'20.7''$
Right ascension(J2000)[B]:	04h16m09.6s
Declination(J2000)[B]:	$-24^{\circ}03'59.7''$
Redshift(blue,red):	3.2840,3.2928 (± 0.0006)
L(Ly α) blue (erg s^{-1}):	$(4.4 \pm 0.1) \times 10^{42} \text{ erg s}^{-1}$
L(Ly α) red (erg s^{-1}):	$(3.7 \pm 0.1) \times 10^{42} \text{ erg s}^{-1}$
Galaxy counterparts	
#1439(SFR; Mass)	$1.5M_{\odot} \text{ yr}^{-1}; 4.4 \times 10^8 M_{\odot}$
#1443(SFR; Mass)	$1.2M_{\odot} \text{ yr}^{-1}; 3.0 \times 10^9 M_{\odot}$
#1485(SFR; Mass)	$3.4M_{\odot} \text{ yr}^{-1}; 1.5 \times 10^{10} M_{\odot}$

2 MUSE INTEGRAL FIELD SPECTROSCOPY

2.1 Hubble Ultra Deep Field and Hubble Frontier Fields MACS J0416

The MUSE instrument mounted on the VLT (Bacon et al. 2012), is an efficient integral field spectrograph highly suitable to blindly look for extended line emission. Its relatively large field of view (1 arcmin^2), spectral range (4750-9350 Å), relatively high spatial ($0.2''$) and spectral ($R \sim 3000$) resolution, and stability allowed us to discover extended Ly α emission, down to faint flux levels.

MUSE observations (Prog. ID 094.A-0289, P.I. Bacon) of the Hubble Ultra Deep Field (Beckwith et al. 2006) were obtained between October and December 2014. Data have been reduced using the standard ESO pipeline version 1.2.1. The raw calibration and science exposures of each single night have been processed, and combined into the final data cube (see Caminha et al. 2016 for a more specific description). The seeing conditions were good, with an average of $\simeq 0.8''$, and 81% of the raw frames with seeing $< 1''$ based on the DIMM monitor at Paranal (the lack of bright stars in the pointing did not allowed us to directly measure the seeing on MUSE data). Moreover, a visual inspection of all exposures (50 with DIT=1500s) from the stacked data cubes did not show evidence of significant variations in observational conditions. We obtain a reduced datacube centered at RA=03h32m38s, DEC= $-27^{\circ}46'44''$ of 19.5 hours total integration time. We identified a spatially extended Ly α emission $\simeq 8'' \times 4''$ wide ($\simeq 70 \times 40$ proper kpc) at $z = 3.32$ in the HUDF centered at coordinates RA=03h32m39.0s, DEC= $-27^{\circ}46'17.0''$. The spectral line profile shows two

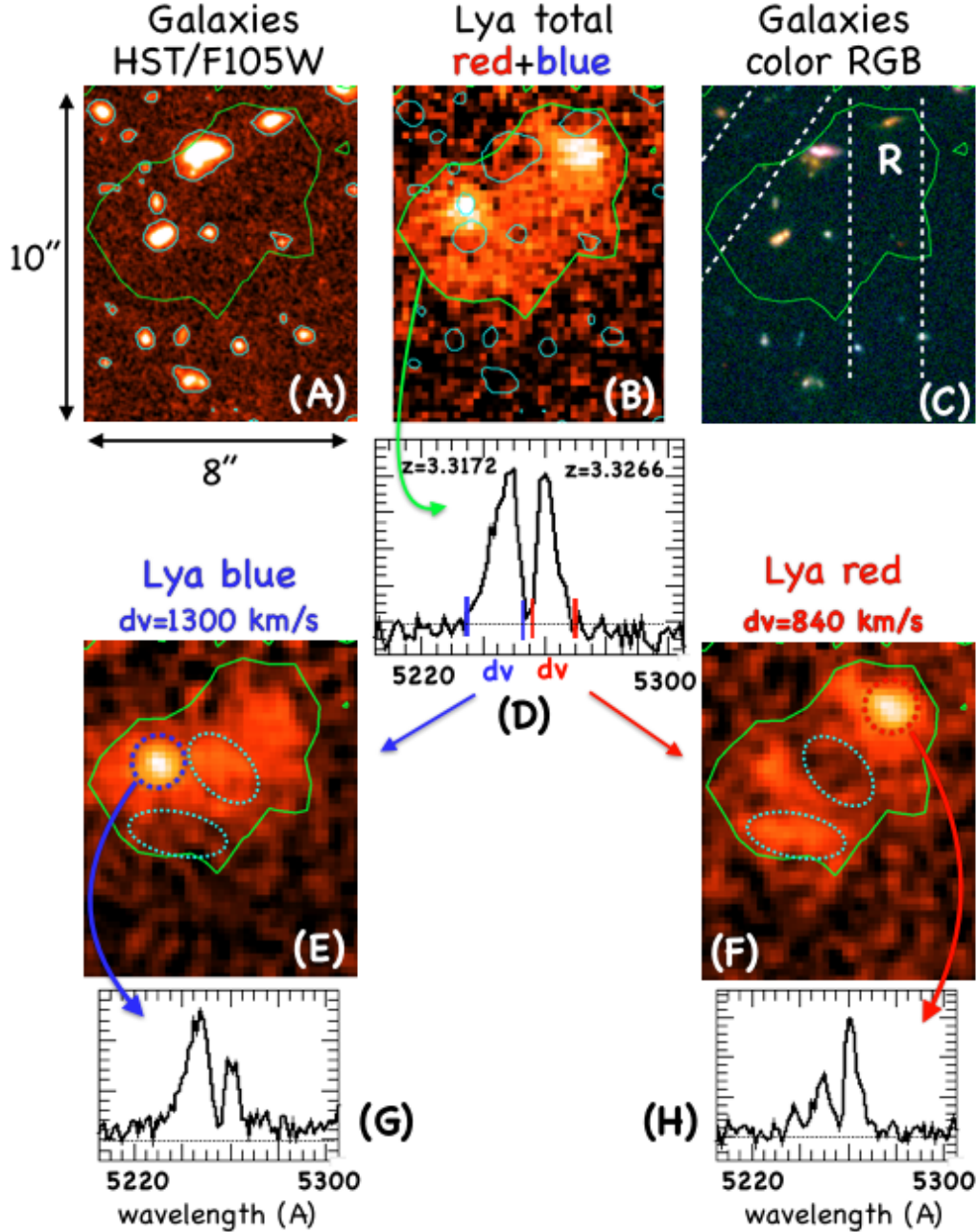


Figure 1. Panel A: HST F105W-band image of the region covering the Ly α nebula. Galaxies are highlighted with contours (only for eye-guidance). Panel B: Ly α nebula as the sum of the two Ly α peaks, blue and red. Contours indicate the position of galaxies, the green contour marks the Ly α emission above 2-sigma from the background. Panel C shows the color image derived from the HST/ACS F435W, F606W, and z850LP bands. Panel D: summed (red + blue) one-dimensional Ly α spectral profile integrated within the green contour, where two peaks are evident. The Ly α spatial maps of the blue and red components are shown in panels E and F, respectively. These are computed by collapsing the signal in the velocity intervals $dv=1300$ and 840 km s^{-1} (marked with blue and red segments). Clearly, the blue and red peaks of the Ly α emission originate from two different, spatially separated regions. The Ly α one-dimensional spectra extracted over these two regions are shown in panels G and H. These spectra are extracted adopting circular apertures of $1.2''$ diameter (blue and red dotted circles). Dotted ellipses mark two regions over which each of the peaks of the Ly α emission either dominates or is depressed.

main peaks, named “red” and “blue”, hereafter, separated by a trough at $z \simeq 3.322$.

MACS J0416 (Lotz et al. 2014; Koekemoer et al. 2014)¹. Data have been taken as part of the GTO program 094.A-0115 (P.I. Richard).

We also analysed MUSE data obtained on the North-Eastern portion of the Hubble Frontier Fields cluster

¹ <http://www.stsci.edu/hst/campaigns/frontier-fields/>

Observations were obtained in November 2014, for a total of 2 hours splitted in 4 exposures. Data have been reduced as described above (and we defer the reader to Caminha et al. 2016 for details) and produced a datacube of 2.0 hours total integration time, centered at RA=04h16m09.95s, DEC=-24°04′01.9″ with position angle 45°. Also in this field we identified a strongly lensed Ly α nebula at $z = 3.33$ with a size of $\simeq 40$ kpc proper with a spectral shape remarkably similar to the one discovered in the HUDF. Two multiple images of the lensed nebula have been identified at coordinates RA=04h16m10.8s, DEC=-24°04′20.5″ and RA=04h16m09.6s, DEC=-24°04′00.0″.

In the following we focus on the details of these two systems. The basic properties are reported in Table 1.

3 LY α EMITTING NEBULA IN THE HUBBLE ULTRA DEEP FIELD

3.1 Previous long-slit spectroscopy

A portion of the the system studied in this work was observed with extremely deep, blind long-slit spectroscopy (Rauch et al. 2011) and, recently, with additional long slit observations (Rauch et al. 2016). Rauch et al. reported a complex structure, i.e., diffuse, fan-like, blue-shifted Ly α emission and a DLA system in front of galaxy R (see Figure 1, top-right). Various scenarios have been discussed, in particular the Ly α emission can be explained if the gas is inflowing along a filament behind the galaxy 'R' (see Figure 1, in which their slit orientations are shown, panel C) and emits fluorescent Ly α photons induced by the ionizing flux escaping from the galaxy.

Long-slit spectroscopy, however, probe only a small volume and offer a marginal/limited view of the whole system. Our study benefit from a number of other key improvements over previous works: (i) the large field of view and spectral resolution of the MUSE instrument is essential for capturing many galaxies simultaneously in a single ultra-deep pointing; (ii) deep HST imaging observations cover the full MUSE field of view; (iii) homogeneous sub-arcsec spatial resolution for all objects is available. In the following we describe the system as observed with MUSE.

3.2 Ly α nebula properties

Using the MUSE datacube we constructed “pseudo-narrowband” (NB) images of the extended emission, centered on the position and wavelength of the corresponding Ly α line.

Before extracting the NB images we performed an additional preprocessing as described in the following. At the low flux levels of interest in this study, source crowding becomes a serious issue for many objects. Several close neighbours within a few arcsec in projection are visible in the HST data. Since these neighbours are typically foreground sources, they contaminate the NB signal only with their continuum emission. A conventional method to remove the contaminating continuum is to subtract a suitably scaled off-band image. We adopted an similar method that fully exploits the information contained in the MUSE datacube: we first median-filtered the datacube in the spectral direction with a very

wide filter window of ± 100 spectral pixels; this produced a continuum-only cube with all line emission removed and with the continuum spectra of real objects being heavily smoothed. The Ly α image has been computed by choosing the band limits such that about 95% of the total line fluxes were included. Being the Ly α nebula double peaked, the bandwidths resulted to be 14 and 9 spectral pixels (1pixel = 1.25Å) for the blue and red Ly α peaks, respectively, corresponding to velocity width of 1300km s $^{-1}$ and 840km s $^{-1}$. We then subtracted this filtered cube from the original data Ly α image and thus obtained an essentially pure emission line cube which was (to first order) free from any continuum signal. As an example the $z = 1.037$ foreground galaxy has been optimally removed (see below). The spatial maps of the red, blue and “red+blue” Ly α nebulae are shown in Figure 1. The integrated Ly α flux computed within a polygonal aperture defined following the green contour of Figure 1 is $(6.1 \pm 0.1) \times 10^{-17}$ erg s $^{-1}$ cm $^{-2}$ and $(4.4 \pm 0.1) \times 10^{-17}$ erg s $^{-1}$ cm $^{-2}$, corresponding to 5.5×10^{42} erg s $^{-1}$ and 4.0×10^{42} erg s $^{-1}$ for the blue and red components, respectively.

4 RESULTS

4.1 Ly α emitting nebula in the UDF

When examining the Ly α emission of this nebula both spatially and spectrally, we identified two main characteristics:

(1) a double-peaked profile in the spectral domain, with blue and red components peaked at redshift 3.3172 and 3.3266 (and $dv = 650$ km s $^{-1}$), each one showing a blue/red tail. The bluer peak is more intense and broader than the red one (FWHM $\sim 520 \pm 50$ km s $^{-1}$ and 280 ± 50 km s $^{-1}$, respectively).

(2) a different overall spatial distribution of the blue and red emission. From the corresponding spatial maps it is evident that the bulk of the emission of the two peaks are segregated (marked with blue/red dotted circles of 1.2″ diameter in Figure 1). Again, the spectral shape of these two selected regions follows the profiles described above (the extracted one-dimensional spectra from the circular apertures are shown in the same figure), in which the strongest blue emission is also broader than the red one.

The ratio of the two peaks depends on the aperture adopted and the position on the nebula. For example, we identified two regions that show a deficit either of blue or red Ly α emission. These are marked with dotted ellipses in Figure 1 (panel E and F). Further details of the spatial behavior of the red and blue emissions along their spectral direction is shown in Figures 2 and 3, in which each slice with step of 1.25Å is shown ($dv = 70$ km s $^{-1}$). In particular the blue emission has been expanded in 13 slices from 5238.75Å to 5253.75Å and appears to grow first from the East side (where it is dominant, e.g., slice 4) and subsequently moves toward the West side following a non-uniform pattern, but maintaining a blue plume over the entire region (slices 10-11). The blue emission covers also regions where the red one is present. The average of all the slices within $dv \simeq 1300$ km s $^{-1}$ is shown in Figure 2.

The red emission has also been expanded in 11 slices from 5255.0Å to 5267.5Å and is mainly located where its main peak has been identified (as discussed above), however

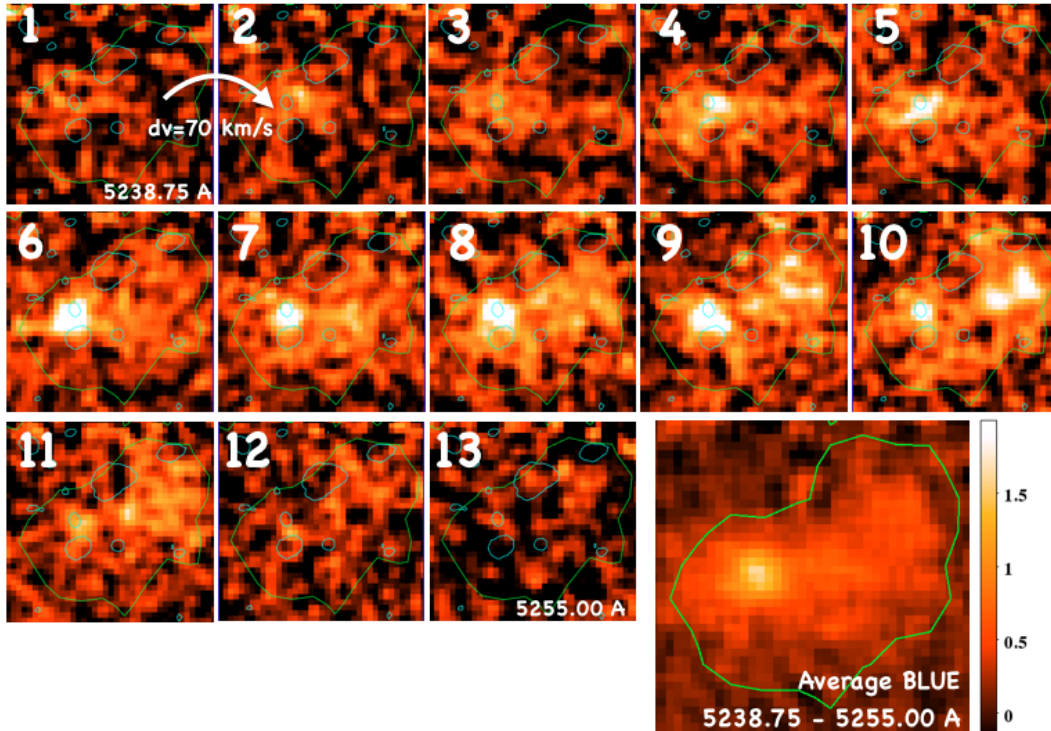


Figure 2. Unpacked images of the blue Ly α component in 13 slices of 1.25\AA each. The images are sorted by progressively increasing wavelength from top-left to bottom-right spanning the range $5238.75\text{\AA} - 5255.00\text{\AA}$. Cyan contours highlight the position of galaxies as shown in Figure 1. A dominant emission is present on the left (East) with an arising plume toward the right-side (West) as wavelength increases. In the bottom-right panel the average of the all slices is shown. The green line indicates the Ly α nebula contour from the “red+blue” map. The color coded bar indicate units of $10^{-20}\text{erg s}^{-1}\text{cm}^{-2}\text{pix}^{-2}$, with $1\text{pix}=0.2''$.

in few slices it shows structures that extend toward the regions where the blue emission is dominant. The average of all the slices within $dv \simeq 840\text{km s}^{-1}$ is shown in Figure 3.

We map the Ly α emission spatially by extracting spectra from apertures covering different regions of the nebula. In particular the one-dimensional profiles are shown in Figure 4, where the two main emissions are shown with blue and red colors. Again, this clearly shows a broader blue component and the different intensities among the two red and blue peaks. It is worth noting that the nebula shows a double peaked Ly α emission from both positions, 1 and 2, marking the blue and red dominant emissions (see Figure 4). The wavelength location of the Ly α trough is not changing significantly, remaining within $d\lambda \simeq 4\text{\AA}$ ($dv \simeq 230\text{km s}^{-1}$) from the central position (5255\AA , $z = 3.3226$), derived by integrating over the entire nebula (green contour in Figure 4).

4.1.1 The broad-band counterparts

We discussed above about the spatial distribution and spectral profile of the emitting Ly α nebula. Here we discuss the identification of possible broad-band counterparts. MUSE integral field spectroscopy allows to extract a $\sim 20\text{hr}$ spectrum of each of the galaxies detected in the HUDF down to the limiting depth. We were able to measure redshifts for 11 galaxies in the region surrounding the nebula, two of them - marked as #7 and #12 - with only tentative redshift estimates (see Figure 5). The MUSE spectra are shown in Figure 6, where the wavelength slices corresponding to the

peak of the most prominent emission line are shown. The redshifts of these galaxies are in the range $1 < z < 6$. No X-ray emission has been detected from the 7Ms Chandra data, neither from the nebula nor from any of the galaxies close by, and no evident high ionization emission lines (e.g., C IV $\lambda 1548, 1550$, He II $\lambda 1640$) have been identified.

Several other galaxies show colors and photometric redshifts (from Coe et al. (2006) and CANDELS ²) consistent with the redshift of the nebula and are reported in Figure 1. Deep VLT/VIMOS U-band (Nonino et al. 2009) and HST/F336W (Rafelski et al. 2015) images are shown in Figure 5. The dropout in these bands of several galaxies further support their high redshift nature. We confirm the presence of a foreground galaxy at $z = 1.037$ and find five additional sources at $z > 3.7$, which are certainly not associated with the nebula. The position of a group of galaxies at $z_{\text{phot}} \simeq 2.5$ is also marked in the figure. One of them is spectroscopically confirmed at $z = 2.4462$. As expected, they are also detected in the VIMOS U-band. Three galaxies (namely, #3, #4 and #6) have spectroscopic redshifts within $dz=0.23$ (corresponding to $dv < 16000\text{km s}^{-1}$) from the red or blue Ly α emissions (all redshifts are reported in Figure 5 and 6).

We were not able to confirm the redshift reported by (Rauch et al. 2011, 2016) for the galaxy #10, at $z = 3.344$, in particular we do not detect the He II $\lambda 1640$ emission line they reported. The MUSE spectrum in the expected posi-

² https://rainbowx.fis.ucm.es/Rainbow_navigator_public/

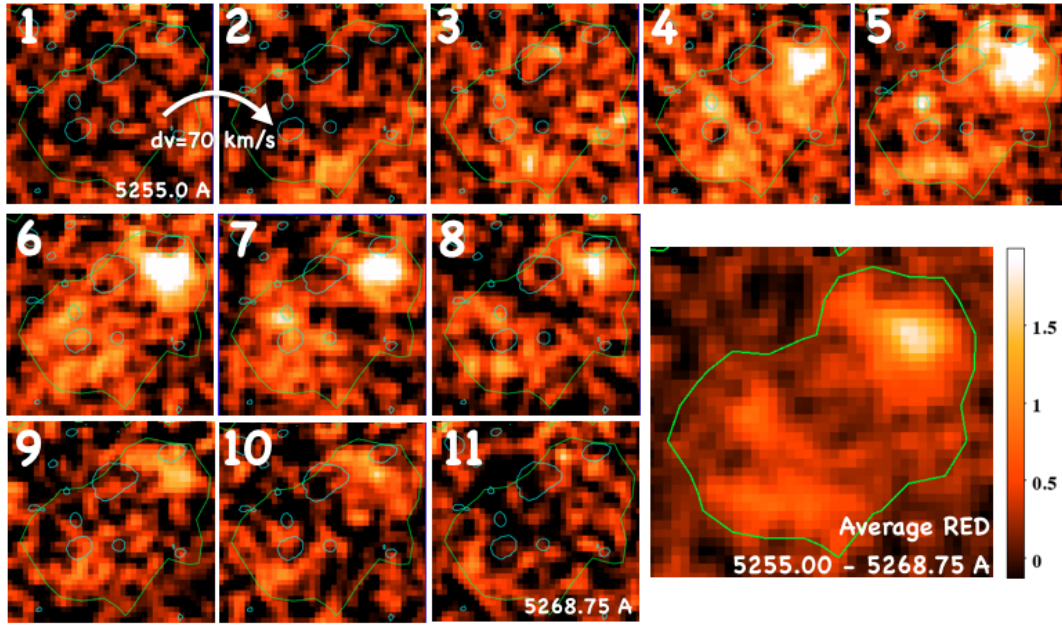


Figure 3. Unpacked images of the red Ly α component in 11 slices of 1.25\AA each. The images are sorted by progressively increasing wavelength from top-left to bottom-right spanning the range $5255.00\text{\AA} - 5268.75\text{\AA}$. Cyan contours highlight the position of galaxies as shown in Figure 1. A dominant emission is present on the right (West) with structure extending toward the left side (East). In the bottom-right panel the average of the all the slices is shown. The green line indicates the Ly α nebula contour from the "red+blue" map. The color coded bar indicate units of $10^{-20} \text{erg}^{-1} \text{s}^{-1} \text{cm}^{-2} \text{pix}^{-2}$, with $1\text{pix}=0.2''$.

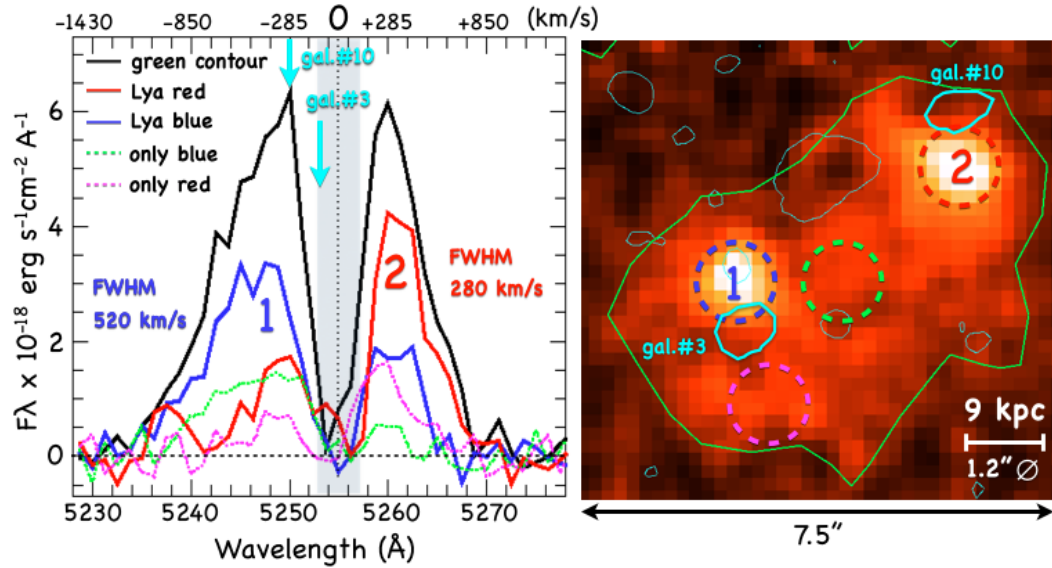


Figure 4. **Right Panel:** the position of four circular apertures ($1.2''$ diameter) are shown on the image of the Ly α nebula (the image shown here is "red+blue"). Green and cyan lines mark the contour of the nebula and galaxies (as described in Figure 1). The two apertures centered on the dominant emissions (1 and 2) are shown in blue and red on the left panel. The galaxy LBG#3 is marked with thick cyan contour and its velocity position relative to the nebula is shown in the left panel. **Left Panel:** The one-dimensional Ly α profiles extracted from the apertures indicated on the right panel. In particular the total profile (extracted from the green contour) is shown in black, and the spectra arising from the apertures 1 and 2 on top of the main emissions are shown in blue and red, respectively (the FWHM are also indicated). Dotted magenta and green lines mark the Ly α profiles in regions where the blue and red emission are deficient, respectively. In general, the double peaked Ly α emission persist over the nebula with the position of the trough consistent with the marked gray region, $\simeq 230 \text{km s}^{-1}$ wide.

tion of HeII λ 1640 is free from sky lines (see Figure 7), and does not show evident line emission down to $3 \times 10^{-18} \text{ erg s}^{-1} \text{ cm}^{-2}$ at 3-sigma level. While the galaxy is a clear U-band dropout with photometric redshifts 3.556 (Coe et al. 2006), and 3.339 (CANDELS), and consistent with the other galaxies and nebula discussed here, we consider the redshift still uncertain. Even adopting the redshift reported by (Rauch et al. 2016), the galaxy would be at 1200 km s^{-1} therefore a possible Ly α emission line would appear redward of the reddest peak of the nebula.

We noted another galaxy presenting a multi-blob morphology, close ($< 0.3''$) to the $z = 1.037$ foreground galaxy and toward the south-east. This object is not recovered by any public photometric catalog, neither CANDELS (Guo et al. 2013) nor GOODS-ACS (Giavalisco et al. 2004). Additionally, this “multi-blob” object is a U-band dropout, as can be inferred from the high spatial resolution deep HST/F336W-band imaging, therefore it is plausibly at $z \gtrsim 3$. We tentatively identified an emission line at 5747 \AA that, if interpreted as Ly α , would place the source at $z = 3.727$. Interestingly, the emission appears spatially resolved suggesting it could be another Ly α blob behind the $z=3.2$ nebula discussed here (this putative blob is marked with red dotted line in Figures 5 and 6). Another galaxy (#8) has been confirmed at the same redshift ($z=3.7267$) of this second blob. When focusing on this $z=3.7$ emission superimposed to the HUDF nebula, another Ly α nebula emerges at $11''$ from it, in the south-east at $z = 3.7123$ with extension $30 \times 20 \text{ kpc}$ physical. We do not discuss further this projected higher redshift Ly α halos, neither the second system at $11''$, and focus on the $z = 3.2$ nebula.

The two-dimensional MUSE snapshots (slices of 1.25 \AA bin) at the wavelength of the main peak of the identified lines are shown in Figure 6, together with their one-dimensional zoomed spectra. The reported IDs are the same of Figure 5. In general, line emissions are evident and the spectral resolution ($R \simeq 1800$) is sufficient to detect the low redshift [OII] λ 3727, 3729 doublet (e.g., galaxy #11, other than $H\gamma$) and the asymmetric profile typical of the high- z Ly α lines. Only for one galaxy (#3, the brightest with $z_{850} = 25.37$) the continuum and several absorption lines have been identified together with the CIII] λ 1907, 1909 emission (this emission is shown in Figure 6). Interestingly, two more line emitters have been identified at the same wavelength and associated to two faint galaxies identified by Coe et al. (2006) with magnitude $z_{850} = 30.59 \pm 0.34$ and 30.75 ± 0.52 (detected at 2 and 3 sigma, respectively; they are shown in the bottom-right panel of Figure 6). The lines are reasonably well detected ($S/N \sim 5 - 7$). One of the two is possibly asymmetric resembling the typical Ly α shape. If the lines are Ly α at $z = 5.133$, they are obviously not associated with the system studied in this work. However, the detection of such a faint spectral feature from galaxies that are so faint to be barely detected even at the HUDF depth, further supports the capability of the MUSE instrument of detecting possible faint counterparts also at the redshift of the nebula.

It is worth noting other two Ly α emissions identified at $\simeq 150 \text{ kpc}$ and 60 kpc proper from the nebula and at the same redshift of the red Ly α component. Figure 8 shows the positions of these emissions compared with the position of the underlying galaxies, whose photometric redshift is also reported. The additional emission lines are consistent with

the photometric redshifts of the closest galaxies, whose magnitudes ranges between 27 up to 30.8 in the z_{850} band. The Ly α emission appears slightly spatially offset from the reported galaxies, possibly due to radiative transfer effects (see Figure 8).

In the following we focus on the closest galaxies possibly related to the Ly α system.

4.1.2 The dominant blue and red Ly α emissions and galaxy counterparts

Three galaxies have been spectroscopically confirmed at redshift 3.3210 (#3), 3.1855 (#6) and 3.0855 (#4) at $< 4''$ from the main blue emission of the nebula, corresponding to few proper kpc transverse ($1'' = 7.6 \text{ kpc}$ proper). Another galaxy, #10, has been plausibly confirmed at redshift 3.3185 close to the red emission. We describe them more in detail in the following.

(i) **Galaxy #3:** Given its redshift ($z = 3.3210$), this is the galaxy that is closest to the nebula in the velocity space with a $dz=0.0016$ from the estimated Ly α trough, corresponding to $dv \simeq 110 \text{ km s}^{-1}$ in the rest-frame of the nebula. This galaxy is spatially resolved and shows a well detected continuum with several ultraviolet low-ionization absorption lines in the MUSE spectrum, e.g., [SiII] λ 1260, [OI] λ 1303 and [CII] λ 1334 (see Figures 5 and 6). The estimated stellar mass is $1.2 \times 10^9 M_{\odot}$ with a star formation rate of $46 M_{\odot} \text{ yr}^{-1}$ (the resulting physical parameters are reported in Figure 9). The [CII] λ 1334 emission has also been detected and provides an estimate of the systemic redshift that is fully compatible with the trough of the Ly α nebula (see Figure 4). Given the redshift and the angular separation from the main blue Ly α peak ($1''$), this galaxy is the closest spectroscopically-confirmed source located at a few tens of physical kpc from the Ly α system. Interestingly, this galaxy is well detected in the HAWKI-Ks band (Fontana et al. 2014) with a magnitude 24.13 at $S/N \simeq 40$, about 1.0 and 0.6 magnitudes brighter than the adjacent HST/F160W and Sptitzer/IRAC $3.6 \mu\text{m}$ bands with magnitudes 25.10 and 24.73 detected at $S/N \gtrsim 40$ and $S/N \simeq 3$, respectively. This discontinuity in the Ks-band strongly suggests the presence of intense [O III] λ 4959, 5007 and $H\beta$ nebular emission lines (see the best SED fitting in Figure 9). Indeed, the result from the SED fitting including nebular prescription produces the best solution with a total equivalent width of $\text{EW}([\text{O III}]\lambda\lambda 4959, 5007 + H\beta) = 1000 \text{ \AA}$. Interestingly, the relatively weak interstellar absorption lines (especially [CII] λ 1334) the CIII] λ 1908 emission, and the strong optical rest-frame Oxygen emissions traced by the broad-band Ks magnitude, resemble the properties recently identified by Vanzella et al. (2016) in a Lyman continuum emitter at similar redshift $z = 3.2$ (see also de Barros et al. 2016). We discuss below the possible link between escaping ionizing radiation and the surrounding gas.

(ii) **Galaxy #6:** this is a rather faint ($z_{850}=27.55$), compact, and low-mass galaxy with stellar mass $3.2 \times 10^7 M_{\odot}$ showing an extremely blue ultraviolet slope ($\beta = -2.55$). The SED fitting suggest a low dust extinction, $A_V = 0.1$, a $\text{SFR}=0.3 M_{\odot} \text{ yr}^{-1}$. The prominent Ly α emission is consistent with the young ages inferred for the burst (10^7 yr). The Ly α line also shows a relatively narrow double peaked

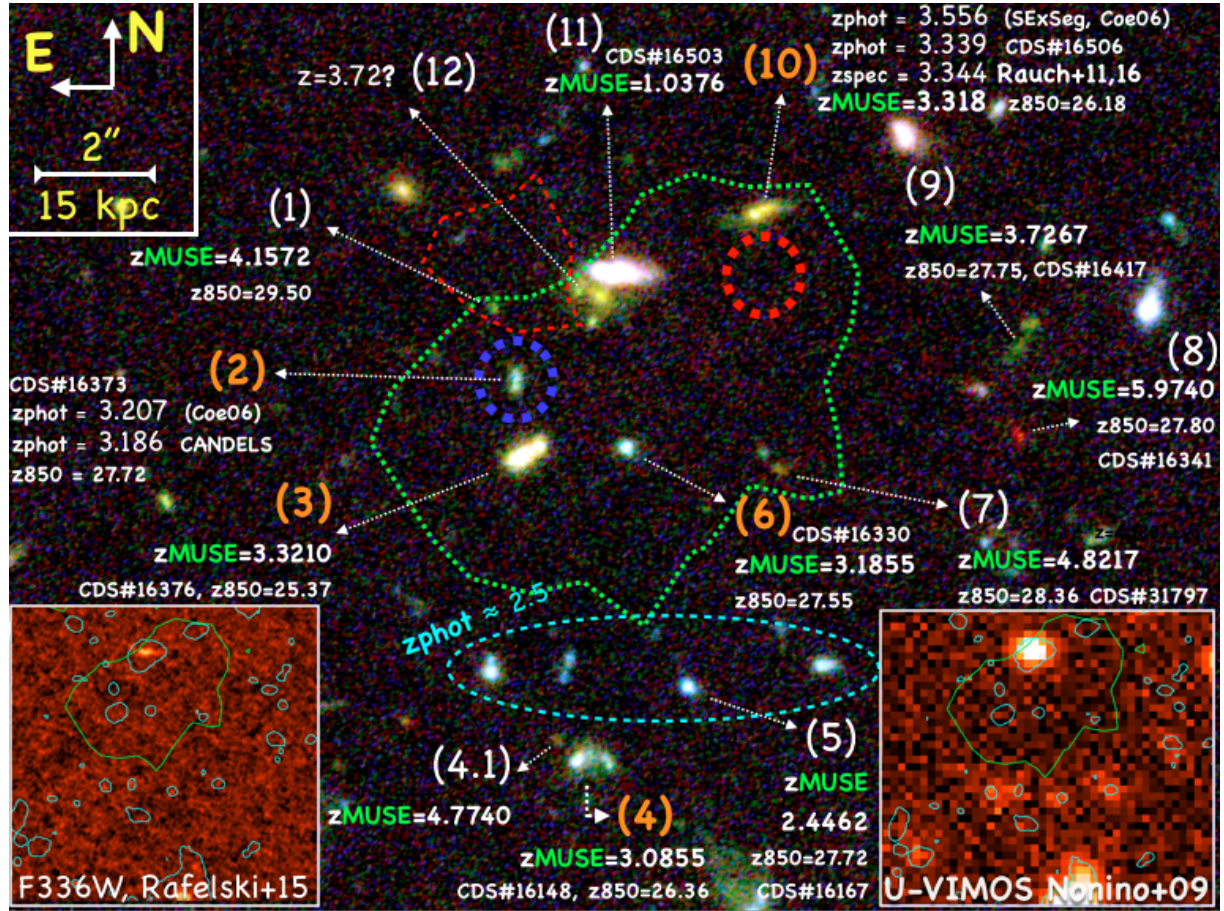


Figure 5. Galaxies surrounding the $\text{Ly}\alpha$ nebula (dotted green contour) are shown superimposed to the HST color image centered on the nebula (F435W, F606W and i775W, Beckwith et al. 2006). Dashed red and blue circles mark the positions of the dominant $\text{Ly}\alpha$ red and blue emissions, respectively (see also Figure 1, panel B). Redshifts extracted from MUSE are highlighted in green and z_{850} magnitudes derived from Coe et al. (2006). The CANDELS identifier is also reported (CDS#) for relevant sources (in particular the IDs highlighted in orange are those possibly associated to the system, see text). The photometric redshifts are reported, if no reliable features were found in the MUSE datacube (Coe et al. 2006 and CANDELS). In the bottom-left/right the same region of the sky is shown in the deep F336W/U-VIMOS bands. This highlights the drop of the majority of the sources considered in this study, therefore supporting their high redshift nature, $z \gtrsim 3$. Galaxies close to the nebula are marked in orange, in particular galaxy ID=3 lies in the $\text{Ly}\alpha$ trough (see text). The thin-dotted red contour marks a possible $\text{Ly}\alpha$ halo at $z = 3.723$, shown in the bottom left panel of Figure 6.

separation ($dv \simeq 400 \text{ km s}^{-1}$) if compared to the brighter L^* galaxy counterparts of $\text{Ly}\alpha$ nebulae (e.g., Kulas et al. 2012). The small peak separation observed in this source is more in line with recent findings at fainter luminosities, where optically-thin systems have been identified (Vanzella et al. 2016; Karman et al. 2016). Given its measured redshift ($z = 3.1855$), this galaxy might be located in front of the $\text{Ly}\alpha$ system. Interestingly, galaxy #6 is positioned over the region where the red emission is minimal, while the blue still survives (see dotted ellipse in Figure 1).

(iii) **Galaxy #4:** this is another galaxy with prominent $\text{Ly}\alpha$ emission at $z = 3.0855$ (see Figure 6), identified toward the south, at $< 4''$ from the nebula. The inferred stellar mass is $5.5 \times 10^8 M_\odot$ with a $\text{SFR} \simeq 0.1 M_\odot \text{ yr}^{-1}$ (see Figure 9).

The redshift difference between the galaxy and the $\text{Ly}\alpha$ trough is $dz = -0.237$ and corresponds to -16400 km s^{-1} . Therefore this galaxy appears to be located in front of the system.

(iv) **Galaxy #2:** It is worth noting that the blue $\text{Ly}\alpha$ peak is exactly aligned with another faint galaxy with mag-

nitude $z_{850} = 27.72$ (galaxy #2, marked in Figure 5), for which no spectroscopic redshift has been measured from MUSE, unless the strong blue $\text{Ly}\alpha$ emission of the nebula contains also the $\text{Ly}\alpha$ of the galaxy. Unfortunately it is not possible to clarify this issue with the current data. The photometric redshift is, however, very close to the redshift of the nebula and the estimated stellar mass is $3 \times 10^7 M_\odot$ and young age $\simeq 10^{7-8}$ years, with a relatively blue ultraviolet slope (see Figure 9). As in the case of galaxy #3, discussed above, this galaxy has also been detected in the Ks-band (with $\text{S/N}=6$) and it appears one magnitude fainter in the F160W band, while only upper limits are available in the IRAC/3.6 μm and 4.5 μm channels $m > 26$. The presence of intense nebular emission lines ([O III] $\lambda\lambda 4959, 5007$ and H β) is, therefore, expected also in this galaxy. When quantified through the SED fitting, the nebular emission lines should have $\text{EW}=1800 \text{ \AA}$ (see Figure 9). While a confirmation would need dedicated near infrared spectroscopy, such strong nebular emission lines are suggestive of high ionization param-

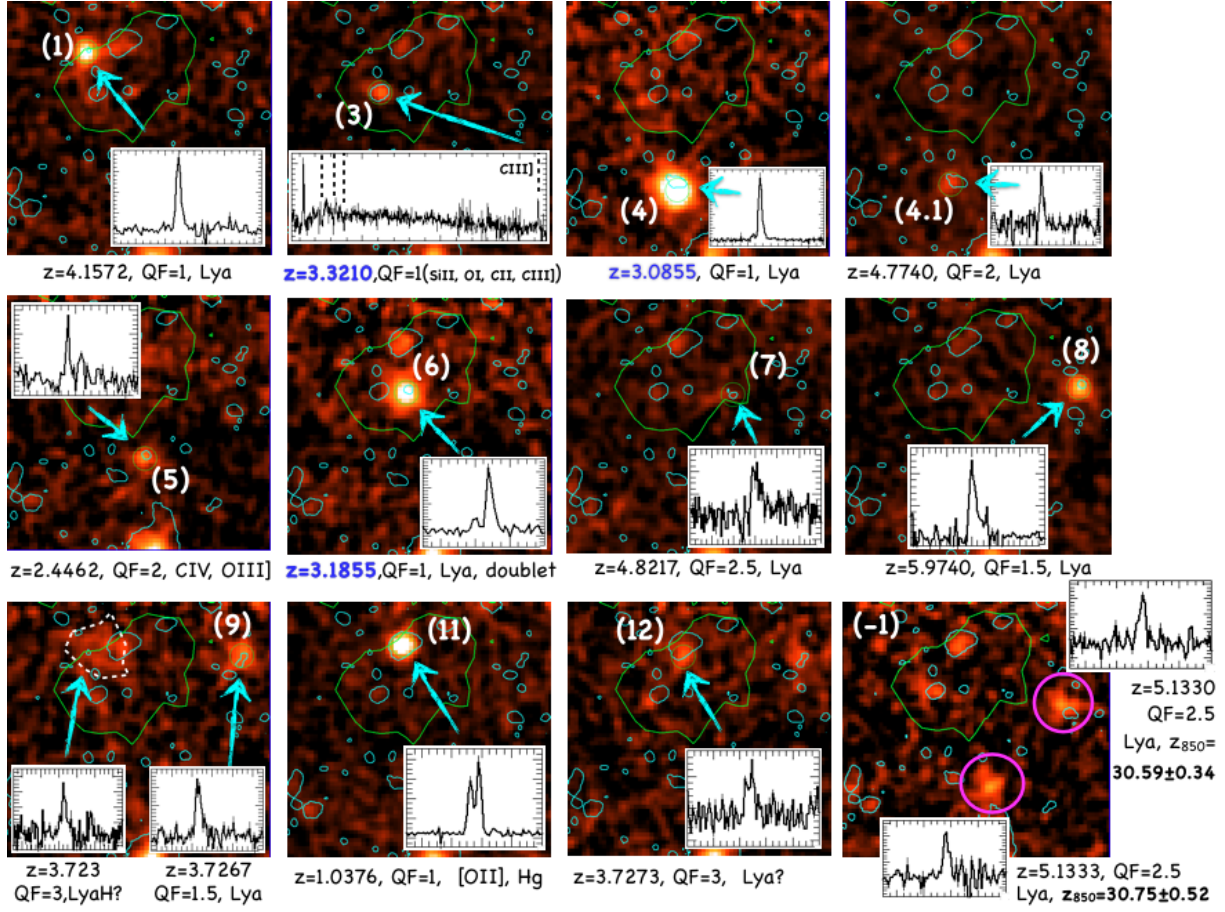


Figure 6. Snapshots of the MUSE spectra ($d\lambda = 1.25\text{\AA}$) of the identified lines. The IDs correspond to the galaxies marked in Figure 5 following from top-left to bottom-right the counterclockwise order. Redshifts are reported in the bottom of each image, with the quality (QF, 1=secure, 2=plausible, 3=tentative) and the main spectral feature identified. In the bottom-right, two emission lines not associate to any CANDELS source are reported. They are consistent with the position of two sources identified by Coe et al. (2006), with magnitudes $z_{850} \gtrsim 30.5$.

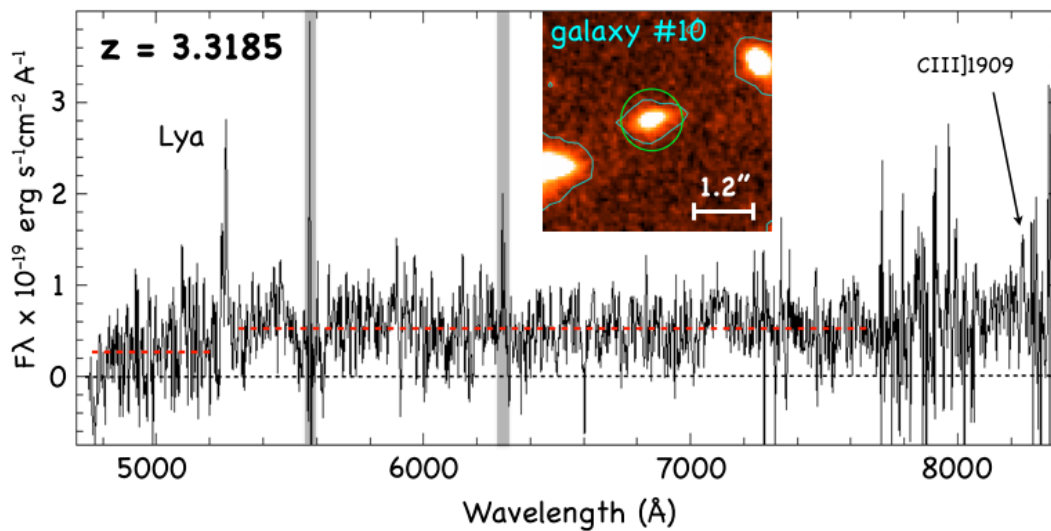


Figure 7. The MUSE spectrum of galaxy #10 calculated within a $1.2''$ diameter aperture (green in the inset) is shown. While no evident absorption lines have been detected, the possible CIII] λ 1907, 1909 in emission and the clear continuum break (marked with dashed red line) are fully compatible with the Ly α emission of the nebula (indicated as Ly α in the figure). The resulting cross correlation produces a redshift $z=3.3185$.

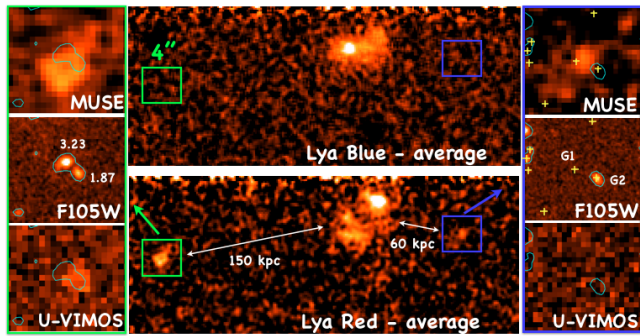


Figure 8. The position of additional Ly α emissions placed at a transverse distance of 150 kpc and 60 kpc proper from the nebula are shown. In the middle top/bottom panels the blu/red emission of the nebula averaged within the velocity slices reported in Figure 1 are shown with marked the additional Ly α emissions. The emissions marked with a green and blue squares at the same wavelength of the red Ly α nebula are evident. In the left and right panels a zoom of these emissions are shown: from top to bottom, the zoomed Ly α emission, the F105W image (with indicated the photometric redshifts from Coe et al. 2006) and the deep U-VIMOS image are shown. Cyan contours mark the position of the galaxies as indicated in Figure 1. In the left panels a galaxy with photometric redshift consistent with the Ly α emission has been identified ($z_{\text{phot}}=3.23$), while the second lower- z object ($z_{\text{phot}}=1.87$) is also detected in the VIMOS U-band (bottom-left image). In the right panels the positions of sources detected in the Coe et al. (2006) catalog (yellow crosses) are also shown. In particular galaxy G1 and G2 have photometric redshifts $z \simeq 3$ and magnitude in the z_{850} -band of 30.80 (S/N=2.8) and 28.81 (S/N=14), respectively.

ters and possible Lyman continuum leakage (e.g., de Barros et al. 2016).

(v) **Galaxy #10:** The main red peak of the nebula has no obvious aligned counterparts. As already discussed above, the closest galaxy is that reported by (Rauch et al. 2011, 2016), here identified as galaxy #10, for which we were not able to confirm Rauch et al. redshift, based on HeII λ 1640 detection at $z = 3.344$ ($\lambda \simeq 7124\text{\AA}$). Figure 7 shown the MUSE spectrum where no clear emission lines have been detected at $\lambda \simeq 7124 \pm 30\text{\AA}$ down to $\simeq 1 \times 10^{-18}\text{erg s}^{-1}\text{cm}^{-2}$ at 3-sigma level. The position of the HeII λ 1640 line is marked with a red arrow in Figure 7 and is free from sky emission lines. Rather, looking more carefully at the MUSE spectrum a continuum break is detected across the Ly α emission. It is not clear if the Ly α (double peaked) emission is coming from the galaxy or is the effect of the seeing that spread the signal into the adopted circular aperture when extracting the MUSE spectrum (marked in green in Figure 7). The cross correlation with typical LBG templates (e.g., Vanzella et al. 2009) including/excluding the Ly α line produces the following solutions, $z=3.3185/3.3127$, respectively (the $z=3.3185$ would also be compatible with possible CIII] λ 1908 line emission). In both cases the redshift is slightly lower than what reported by Rauch et al. and place the galaxy at $-690/-285\text{km s}^{-1}$ from the Ly α trough of the nebula, while the previous redshift, $z=3.344$, would put it at $+1480\text{km s}^{-1}$, even redder than the red peak of the nebula. As discussed by Rauch et al. (2011, 2016) this galaxy together with the other counterparts is probably playing a role in shaping the

profile and morphology of the Ly α nebula. We performed SED fitting also for this galaxy, obtaining a remarkable star formation activity ($\sim 100M_{\odot}\text{yr}^{-1}$) with a stellar mass of $\simeq 10^9M_{\odot}$ (the more massive among the counterparts) and relatively red ultraviolet slope (Figure 9).

4.2 Gravitationally lensed Ly α emitting nebula in the Hubble Frontier Fields MACS J0416

Another strongly magnified Ly α nebula has been discovered at redshift $z = 3.22$ behind the Hubble Frontier Fields MACSJ0416, as a gravitationally lensed system showing two multiple images (see Figure 10). We report about this system because of its very similar spectral properties to the nebula discovered in the HUDF. The size of the emitting gas is smaller than the system discovered in the HUDF, having a lens-uncorrected (i.e., observed) extension of the order of 40 kpc. The two images have been identified at RA=04h16m10.9s, DEC=−24°04′20.7″ (the more magnified image, image A hereafter, with magnification $\mu \simeq 2$) and RA=04h16m09.6s, DEC=−24°03′59.7″ (a second less magnified image, image B hereafter, with $\mu \simeq 1$). This multiple imaged system has been used in the new highly-precise strong lensing model, which uses a large set of new multiple systems spectroscopically confirmed with MUSE (it corresponds to System 9 in Caminha et al. in prep.). The image positions are fully consistent with the strong lensing model, which accurately reproduces their positions. The morphology in the source plane is slightly distorted, but a more careful dedicated modeling would be required to derive meaningful conclusions. That is out of the scope of the present work and it will be presented in a separate dedicated study (Caminha et al. in prep.). We note that also in this case the spatial distribution of Ly α -red and Ly α -blue (especially in image A) are not coincident. This is shown in Figure 10, where the red contours mark the position of the Ly α -red emission, which appears slightly displaced compared to the Ly α -blue emission).

Remarkably, the spectral properties of this nebula are very similar to those of the HUDF nebula discussed above. In particular, the (1) rest-frame velocity difference, (2) line widths (FWHM), and (3) global shape – e.g., the bluer Ly α peak is systematically broader than the red one – are very similar in both nebulae. Figure 11 shows a comparison of the two spectral profiles as they are observed. After correcting the line fluxes by the magnification factor (e.g., $\mu = 2$ for image A), we obtain a Ly α luminosity of $4.4 \times 10^{42}\text{erg s}^{-1}$ and $3.7 \times 10^{42}\text{erg s}^{-1}$ for the blue and red peaks, respectively. The relative peak ratio changes as in the HUDF nebula, showing different regions where either the blue or the red emission dominate.

The multiple images produced by strong lensing allow us to investigate the broad-band counterparts more easily than in the HUDF case. In particular a triplet of galaxies aligned with the emitting gas (Ly α) have been identified. They are visible in both multiple images (A and B) and, therefore, are likely associated to the nebula. If they were at different redshift no multiple images would be produced or they would be significantly offset from the Ly α emission (see Figure 10). It is worth noting that also in the strongly lensed Ly α blob studied by Caminha et al. (2015) there were three

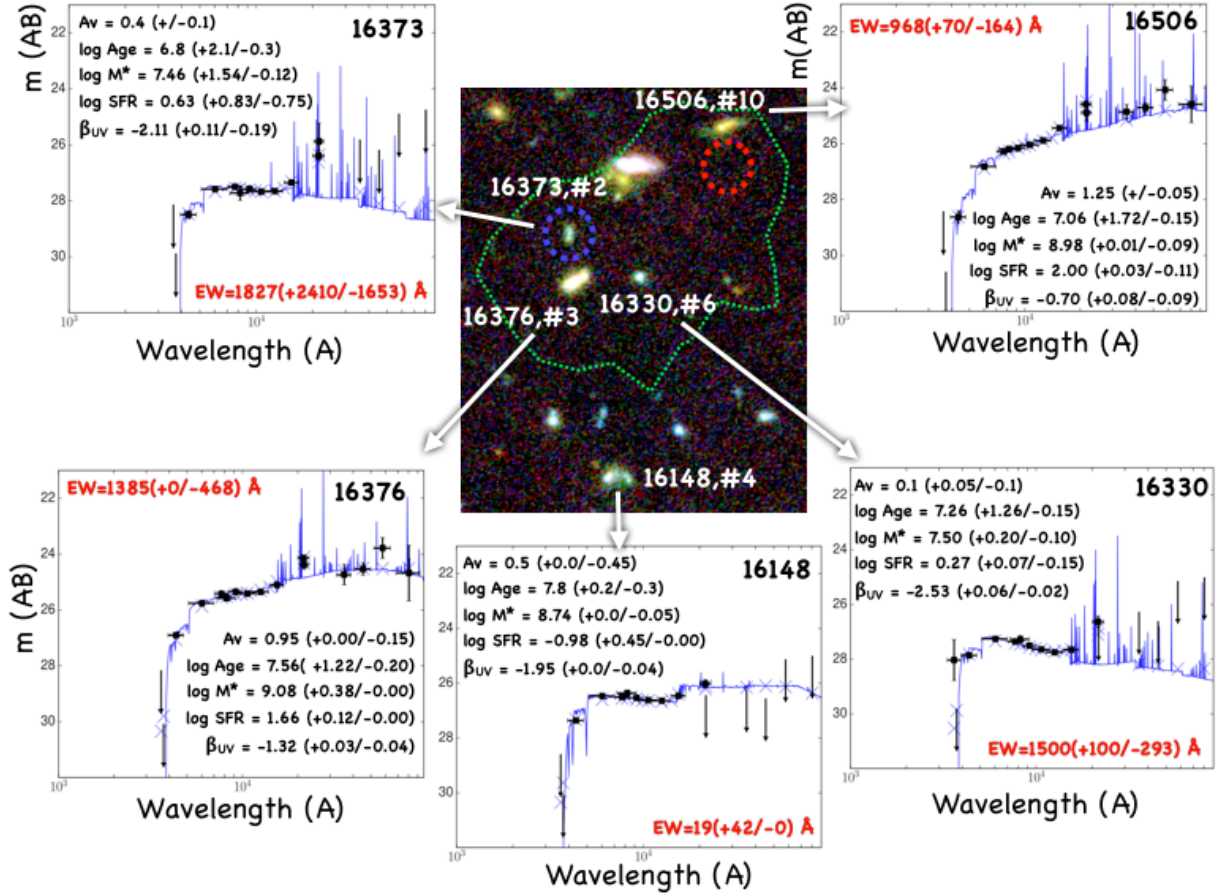


Figure 9. The SED-fitting of the galaxies described in the text and possibly associated to the nebula are shown. The IDs are same used in the previous figures and Table 1. Basic physical quantities are reported in black, while the estimated equivalent width of the group [O III] $\lambda\lambda$ 4959, 5007 and H β is reported in red. Apart from galaxy #4, all the other galaxies show very high equivalent widths. In particular, galaxy #4 is the bluest one of the sample, consistent with a negligible dust attenuation.

aligned star-forming galaxies associated to the emitting gas. The clear double peaked spectral shape of the Ly α emission showing blue and red asymmetries suggest it is not the simple sum of the Ly α emissions arising from each galaxy and blurred by the seeing in the MUSE image. Rather, it appears as a diffuse well resolved emission of $\simeq 4.0 \times 2.5''$ (in the case of image A) detected in a region much larger than the stellar continuum of each galaxy (see black contours in Figure 10).

Other than the Ly α emission, no additional spectral feature (e.g., no high ionisation lines, CIV λ 1548, 1550, OIII λ 1661, 1666, CIII $\lambda\lambda$ 1907, 1909) have been identified in the spectra of these galaxies. Therefore, we assume that these three galaxies are at the redshift of the nebula on the basis of geometrical arguments, and with the support of the lensing model. We checked the photometric redshifts of the three galaxies using the ASTRODEEP photometric redshift catalog recently published by Castellano et al. (2016). All of them are fully consistent with the redshift of the Ly α nebula, $z = 3.2$. More specifically, the three galaxies have ASTRODEEP IDs 1439, 1443 and 1485 and photometric redshift $\simeq 3.55, 3.35$ and 3.45 . Two of them, 1439 and 1443, show relatively low stellar mass $4.4 \times 10^8 M_\odot$ and $3.0 \times 10^9 M_\odot$ and a possible excess in the K-band that would suggest a

strong nebular contribution in this band by the group of lines [O III] $\lambda\lambda$ 4959, 5007 + H β . As discussed above, these features may suggest a possible link with escaping ionizing radiation. The third galaxy, 1485, is the most massive one with $1.5 \times 10^{10} M_\odot$.

The star formation rate of the three objects (1439, 1443, and 1485) has been estimated to be 1.5, 1.2, and $3.4 M_\odot \text{ yr}^{-1}$, respectively (Castellano et al. 2016).

5 DISCUSSION AND CONCLUSIONS

We discovered and discussed two extended Ly α systems at redshift $\simeq 3.3$. The prominent blue peak in their Ly α spectra accompanied by a fainter red, slightly narrower peak is remarkable. Usually, Ly α has been observed with dominant red tails indicative of outflows (e.g., Shapley et al. 2003; Vanzella et al. 2009) as well as many Ly α blobs (e.g., Matsuda et al. 2006). Here we observe the opposite.

This is even more relevant if the intergalactic absorption is considered, that would tend to preferentially suppress the bluer peak. In particular, an IGM transmission in the blue side of the Ly α ranging between 20% and 95% (68% interval)

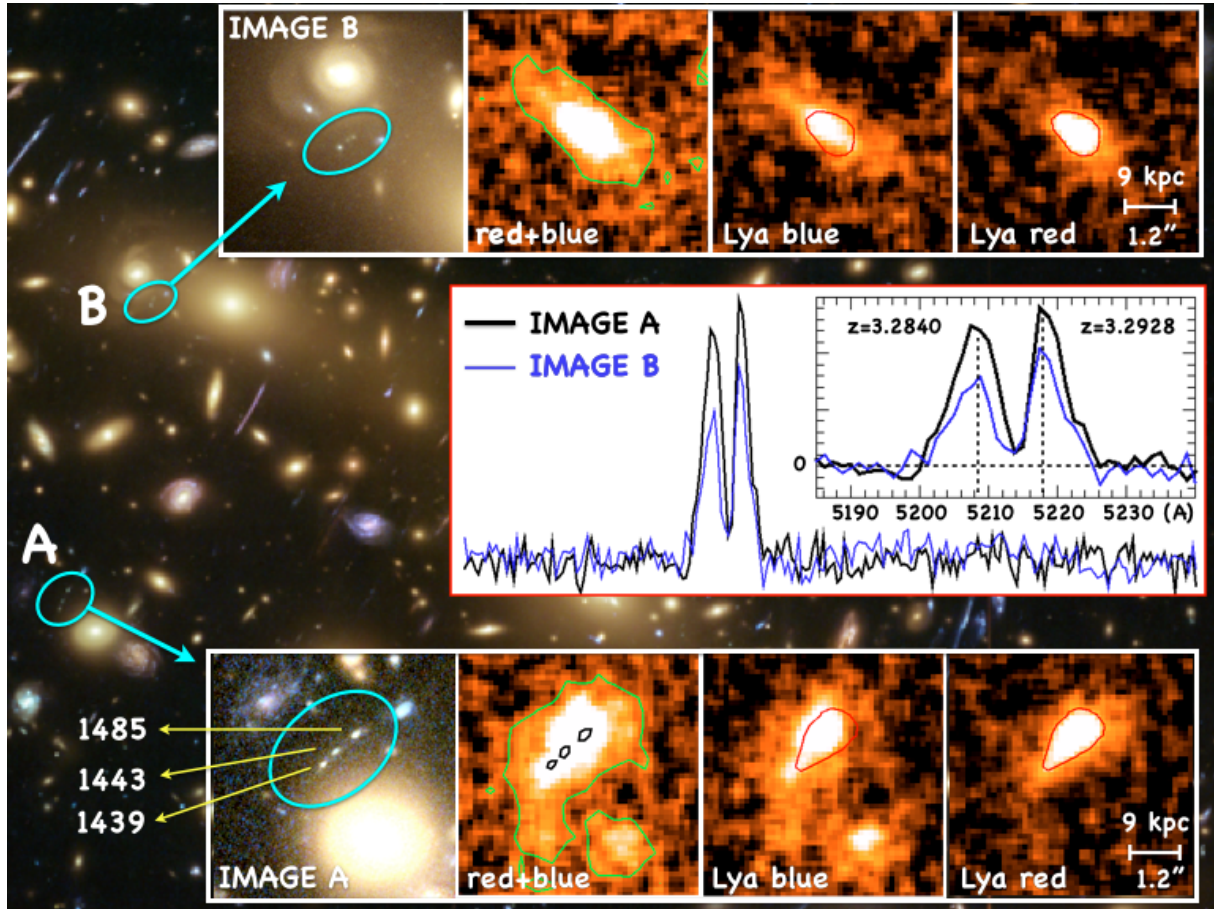


Figure 10. The lensed Ly α nebula discovered behind the Hubble Frontier Field MACSJ0416 at $z = 3.2$ is shown. Two multiple images have been marked and Ly α spatial distribution is shown in the insets (from left to right: the color image, Ly α “red + blue”, only red and only blue). In the middle inset the spectrum around the Ly α and a zoomed spectral profile are shown for both images, A (thick black line) and B (thick red line). The three galaxies associated to the nebula are marked in the bottom left with yellow arrows and the corresponding IDs from the ASTRODEEP catalog (Castellano et al. 2016).

with a mean of $\sim 80\%$ has been proposed by Laursen et al. (2011).

The Ly α nebulae described in this work benefit of the integral field spectroscopy (MUSE), which is more informative than previous long-slit studies (e.g., Rauch et al. 2016). Despite that, the complexity of the system still prevents us from deriving firm conclusions. So we can at best test the plausibility of the processes involved and discuss the most likely scenarios.

As mentioned above the nebulae described in this work show quite complex structure with spatial-dependent Ly α emission (Figures 2 and 3) and varying sub-spectral profiles (Figure 4), however two clear spectral features are present in both systems: (1) the broad doubled peaked line profile with prominent blue emission and (2) the ‘trough’ separating the two peaks which appears to occur mostly at the same frequency throughout the nebula (this is best illustrated by the left panel of Figure 4). These two observations combined can be naturally explained with scattering, and support the fact that radiative transfer effects are likely responsible for shaping the spectra emerging from these nebulae.

The simplest version of the scattering medium consists of a static gas cloud of uniform density. For such a medium,

the emerging Ly α spectrum is double peaked, with the peak separation set by the total HI column density of the cloud (e.g., Harrington 1973; Neufeld 1990; Dijkstra 2014):

$$N_{HI} = 5.3 \times 10^{20} \left(\frac{T}{10^4 K} \right)^{-1/2} \left(\frac{dv}{670 \text{ km s}^{-1}} \right)^3 \text{ cm}^{-2}. \quad (1)$$

However, this possibility has been excluded by Rauch et al. (2011) on the basis of similar spectral properties we find here, e.g., the relatively stronger intensity of the blue versus red emission and the different widths suggests that we are not observing a static configuration. Radiative transfer through clumpy/multiphase media can also explain double peaked spectra (see Gronke & Dijkstra 2016). Clumpy media generally give rise to a wide variety of broad, multi-peaked spectral line profiles. The trough at a constant frequency then reflects either that there is a non-negligible opacity in residual HI in the hot inter clump gas (Gronke & Dijkstra 2016), or in the cold clumps that reside in the hot halo gas (the presence of these clumps inside massive dark matter halos has been proposed by, e.g., Cantalupo et al. 2014 and Hennawi et al. 2015). The width of the trough reflects either the thermal broadening of the Ly α absorption cross-section for residual HI in the

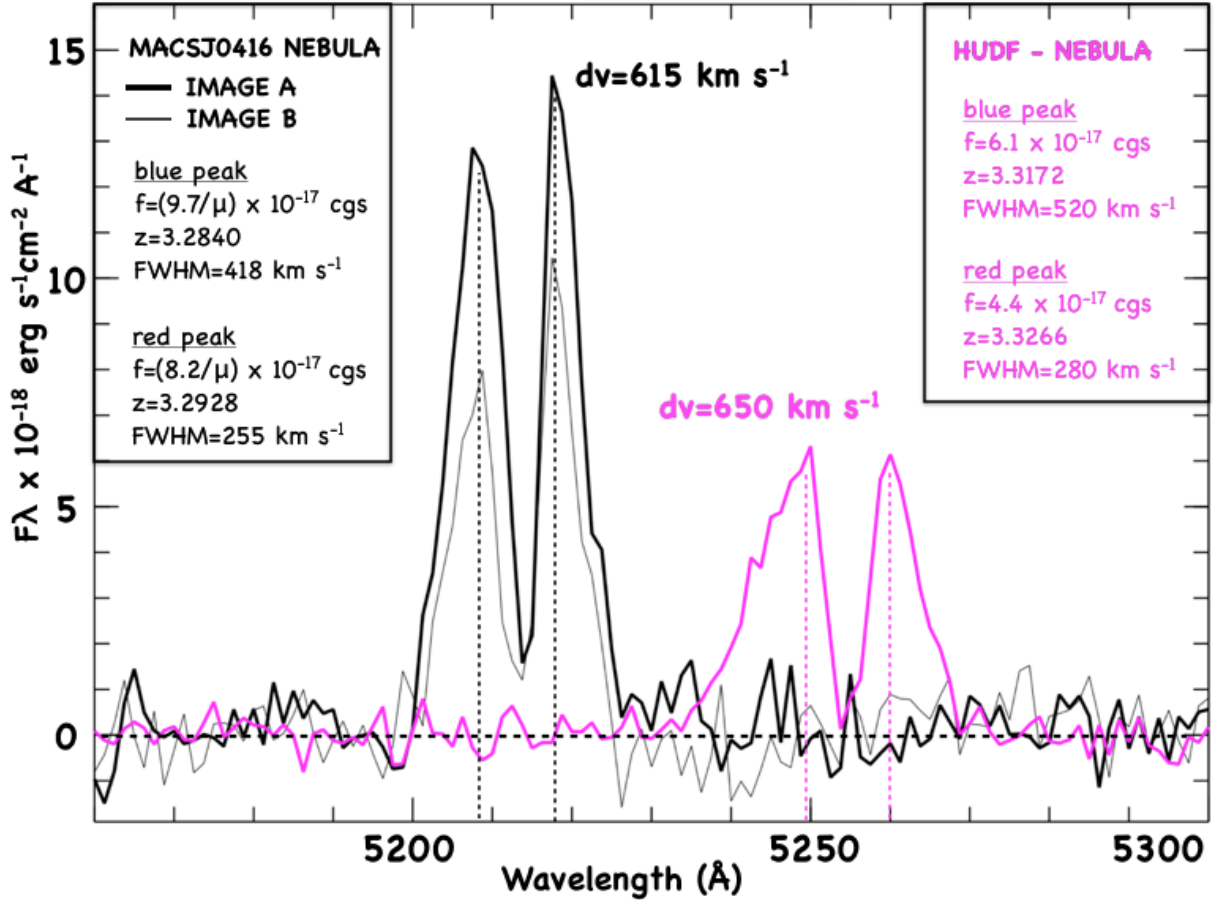


Figure 11. The two Ly α profiles of the nebulae described in this work are shown in the observed wavelength domain. Black thick (thin) line shows the profile for the lensed nebula, image A (B). Relevant parameters are reported. In the case of MACSJ0416 nebula numbers are reported for image A, for which the magnification is $\mu \simeq 2$ (Caminha et al. in prep.). Remarkably, the trough, velocity difference, and widths of the two nebulae are very similar.

hot gas, and/or the velocity dispersion of the cold clumps.

Also the origin of Ly α emission in these nebulae is not easily identifiable.

Star Formation. The association of the brightest Ly α spots with galaxies (in the HUDF nebula) and the three aligned star-forming galaxies in the lensed nebula suggest that star formation is at least powering the Ly α emission from the high-surface brightness spots. The enhancement of the blue and/or red peak in these brighter spots either reflects the kinematics of the clumps surrounding these galaxies, where an enhanced blue (red) peak is indicative of clumps falling onto (flowing away from) the galaxies (see Zheng & Miralda-Escudé 2002; Dijkstra et al. 2006a,b; Verhamme et al. 2006). Alternatively, enhancements in any of the two peaks could be due the galaxies bulk motion with respect to the Ly α emitting nebula (i.e. these could be star-forming galaxies which are moving onto the more massive halo that hosts the Ly α nebula).

Cooling. For massive dark matter halos ($M_{\text{halo}} \sim 1 - 5 \times 10^{12} M_{\odot}$), the cooling luminosity can reach $L \sim 10^{43} \text{ erg s}^{-1}$ (e.g., Dijkstra & Loeb 2009; Faucher-Giguère et al. 2010; Goerdt et al. 2010; Rosdahl

& Blaizot 2012), which is sufficient to explain these halos. The overall double peaked spectrum is reminiscent of that predicted by Faucher-Giguère et al. (2010) for cooling radiation (though see Trebitsch et al. 2016). In particular the observed velocity difference ($\simeq 650 \text{ km s}^{-1}$) and the Ly α total luminosity are compatible to those reported by Faucher-Giguère et al. (2010). Also in terms of spatial emission there are similarities, like the extensions of several tens kpc and the emission arising in different places. The spatial extent results from a combination of some of the cooling radiation being emitted in the accretion streams far from the galaxy(ies), and of spatial diffusion owing to resonant scattering. Also the presence of a well developed blue component slightly broader than the red one is among the outputs of the Faucher-Giguère et al. (2010) prescriptions (see their Figure 5), and is indicative of systematic infall, in which the velocity of the in-flowing gas tend to move (in the frequency domain) the red Ly α photons toward the resonance, while making easier for the blue Ly α photons to escape in the blue side.

Fluorescence. It is also possible that ionising photons escape from galaxies, which would cause the cold clouds to fluoresce in Ly α (e.g., Mas-Ribas & Dijkstra 2016). Flu-

orescent Ly α emission also gives rise to a double peaked spectrum, in which infalling/outflowing material diminishes the red/blue wing of the spectrum. However, fluorescence tend to produce a smaller peak separation than what is observed here (e.g., [Gould & Weinberg 1996](#); [Cantalupo et al. 2005](#)). In other words, if fluorescence is the source of Ly α emission, then we would still need additional scattering to explain the width of the Ly α line. Note that this explanation also relies on star formation powering the Ly α emission. Given the number of galaxies that are possibly associated to each system, this explanation is energetically compatible with the observed star formation activity (see [Rauch et al. 2011](#)). Moreover, as mentioned above, the strong optical rest-frame nebular emission ([O III] $\lambda\lambda$ 4959, 5007 and H β) as traced by the K-band for some of the galaxies (e.g. #3, #2, and #6 in the HUDF nebula and in the lensed nebula) is intriguingly similar to what has been recently observed in a $z = 3.2$ galaxy (with equivalent widths of $\text{EW}([\text{O III}]\lambda\lambda 4959, 5007) = 1500\text{\AA}$, [de Barros et al. 2016](#) and showing a remarkable amount of escaping ionizing radiation (higher than 50%, [Vanzella et al. 2016](#)). Among them it is worth noting the presence of the extremely blue (and in practice dust-free), compact, and low-mass galaxy (#6), that might further contribute to the ionisation budget. The Ly α resonance emission from nebulae may be indirect probes of the escaping ionising radiation from the embedded sources (even fainter than the detection limit), along transverse directions not accessible from the observer. While, the direct detection of Lyman continuum emission is in principle possible, it might be precluded in the present data because galaxies are surrounded by the same (circum-galactic) medium plausibly producing the Ly α nebula and therefore preventing us to easily detect ionising flux. In addition, the intergalactic opacity in the Lyman continuum also affects these measurements (e.g., [Vanzella et al. 2012](#)), requiring a larger sample of similar systems to average the IGM stochastic attenuation.

AGN Activity. AGN can inject large amounts of energy in the surrounding gas (e.g., [Debuhr et al. 2012](#)), which could radiate even after the nucleus has shut off. Such processes can modify the kinematic and thermal properties of the circum-galactic medium, and therefore its Ly α signatures.

The key observable that distinguishes between different sources of Ly α emission would be the Balmer emission lines (like H α or H β). In the case of cooling radiation, the H α flux that is associated with Ly α should be ~ 100 times weaker ([Dijkstra 2014](#)), and would likely be undetectable. However, for the ‘star formation’ and ‘fluorescence’ models, the H α flux should be significantly stronger. If H α emission can be observed, and confined to galaxies then Ly α emission was likely powered by nebular emission inside galaxies, while fluorescence would give rise to partially extended H α .

The search for galaxies that illuminate themselves through some fortuitous release of Ly α or ionizing radiation into their environment offer positive prospects in the future MUSE observations and will provide our main direct insights into the in- and outflows of gas ([Rauch et al. 2016](#)). If the scenario in which the gas is inflowing toward a region forming stars is correct, then we may be witnessing an early phase of galaxy or a proto-cluster (or group) formation. Searches for asymmetric Ly α halos or offsets between stel-

lar populations and Ly α emission may reveal further objects where the escape of ionizing radiation can be studied.

ACKNOWLEDGEMENTS

We thanks F. Calura and G. Zamorani for useful discussions and A. Grazian for providing us the K-band image of the HUDF nebula. Part of this work has been funded through the PRIN INAF 2012.

REFERENCES

- Adelberger, K. L., Steidel, C. C., Shapley, A. E., & Pettini, M. 2003, *ApJ*, 584, 45
- Bacon, R., Accardo, M., Adjali, L., et al. 2012, *The Messenger*, 147, 4
- Beckwith, S. V. W., Stiavelli, M., Koekemoer, A. M., et al. 2006, *AJ*, 132, 1729
- Borisova, E., Cantalupo, S., Lilly, S. J., et al. 2016, *arXiv:1605.01422*
- Caminha, G. B., Karman, W., Rosati, P., et al. 2015, *arXiv:1512.05655*
- Cantalupo, S., Porciani, C., Lilly, S. J., & Miniati, F. 2005, *ApJ*, 628, 61
- Cantalupo, S., Arrigoni-Battaia, F., Prochaska, J. X., Hennawi, J. F., & Madau, P. 2014, *Nature*, 506, 63
- Castellano, M., Amorín, R., Merlin, E., et al. 2016, *A&A*, 590, A31
- Chen, H.-W., Lanzetta, K. M., Webb, J. K., & Barcons, X. 2001, *ApJ*, 559, 654
- Christensen, L., Sánchez, S. F., Jahnke, K., et al. 2004, *A&A*, 417, 487
- Coe, D., Benítez, N., Sánchez, S. F., et al. 2006, *AJ*, 132, 926
- de Barros, S., Vanzella, E., Amorín, R., et al. 2016, *A&A*, 585, A51
- Debuhr, J., Quataert, E., & Ma, C.-P. 2012, *MNRAS*, 420, 2221
- Dijkstra, M., Haiman, Z., & Spaans, M. 2006, *ApJ*, 649, 37
- Dijkstra, M., Haiman, Z., & Spaans, M. 2006, *ApJ*, 649, 14
- Dijkstra, M., & Loeb, A. 2009, *MNRAS*, 400, 1109
- Dijkstra, M. 2014, *Publ. Astron. Soc. Australia*, 31, e040
- Faucher-Giguère, C.-A., Kereš, D., Dijkstra, M., Hernquist, L., & Zaldarriaga, M. 2010, *ApJ*, 725, 633
- Fontana, A., Dunlop, J. S., Paris, D., et al. 2014, *A&A*, 570, A11
- Francis, P. J., Dopita, M. A., Colbert, J. W., et al. 2013, *MNRAS*, 428, 28
- Gialvalisco, M., Vanzella, E., Salimbeni, S., et al. 2011, *ApJ*, 743, 95
- Goerdt, T., Dekel, A., Sternberg, A., et al. 2010, *MNRAS*, 407, 613
- Gould, A., & Weinberg, D. H. 1996, *ApJ*, 468, 462
- Gronke, M., & Dijkstra, M. 2016, *arXiv:1604.06805*
- Guo, Y., Ferguson, H. C., Gialvalisco, M., et al. 2013, *ApJS*, 207, 24
- Hayes, M., Scarlata, C., & Siana, B. 2011, *Nature*, 476, 304
- Hennawi, J. F., Prochaska, J. X., Cantalupo, S., & Arrigoni-Battaia, F. 2015, *Science*, 348, 779
- Harrington, J. P. 1973, *MNRAS*, 162, 43
- Lanzetta, K. M., Bowen, D. V., Tytler, D., & Webb, J. K. 1995, *ApJ*, 442, 538
- Laursen, P., Sommer-Larsen, J., & Razoumov, A. O. 2011, *ApJ*, 728, 52
- Lotz, J., Mountain, M., Grogin, N. A., et al. 2014, *American Astronomical Society Meeting Abstracts #223*, 223, 254.01

- Karman, W., Caputi, K. I., Caminha, G. B., et al. 2016, arXiv:1606.01471
- Koekemoer, A. M., Avila, R. J., Hammer, D., et al. 2014, American Astronomical Society Meeting Abstracts #223, 223, 254.02
- Kulas, K. R., Shapley, A. E., Kollmeier, J. A., et al. 2012, ApJ, 745, 33
- Martin, D. C., Matuszewski, M., Morrissey, P., et al. 2015, Nature, 524, 192
- Mas-Ribas, L., & Dijkstra, M. 2016, ApJ, 822, 84
- Matsuda, Y., Yamada, T., Hayashino, T., Yamauchi, R., & Nakamura, Y. 2006, ApJ, 640, L123
- Neufeld, D. A. 1990, ApJ, 350, 216
- Nonino, M., Dickinson, M., Rosati, P., et al. 2009, ApJS, 183, 244
- Patrício, V., Richard, J., Verhamme, A., et al. 2016, MNRAS, 456, 4191
- Prescott, M. K. M., Dey, A., Brodwin, M., et al. 2012, ApJ, 752, 86
- Prescott, M. K. M., Martin, C. L., & Dey, A. 2015, ApJ, 799, 62
- Rafelski, M., Teplitz, H. I., Gardner, J. P., et al. 2015, AJ, 150, 31
- Rauch, M., Becker, G. D., Haehnelt, M. G., et al. 2011, MNRAS, 418, 1115
- Rauch, M., Becker, G. D., & Haehnelt, M. G. 2016, MNRAS, 455, 3991
- Rosdahl, J., & Blaizot, J. 2012, MNRAS, 423, 344
- Shapley, A. E., Steidel, C. C., Pettini, M., & Adelberger, K. L. 2003, ApJ, 588, 65
- Steidel, C. C., Erb, D. K., Shapley, A. E., et al. 2010, ApJ, 717, 289
- Swinbank, A. M., Vernet, J. D. R., Smail, I., et al. 2015, MNRAS, 449, 1298
- Trebitsch, M., Verhamme, A., Blaizot, J., & Rosdahl, J. 2016, arXiv:1604.02066
- Turner, M. L., Schaye, J., Steidel, C. C., Rudie, G. C., & Strom, A. L. 2014, MNRAS, 445, 794
- Vanzella, E., Giavalisco, M., Dickinson, M., et al. 2009, ApJ, 695, 1163
- Vanzella, E., Guo, Y., Giavalisco, M., et al. 2012, ApJ, 751, 70, 70
- Vanzella, E., de Barros, S., Vasei, K., et al. 2016, ApJ, 825, 41
- Verhamme, A., Schaerer, D., & Maselli, A. 2006, A&A, 460, 397
- Wisotzki, L., Bacon, R., Blaizot, J., et al. 2016, A&A, 587, A98
- Zheng, Z., & Miralda-Escudé, J. 2002, ApJ, 578, 33

This paper has been typeset from a \LaTeX file prepared by the author.